Single-Molecule Conductance of Redox Molecules in Electrochemical Scanning Tunneling Microscopy †

ARTICLE *in* THE JOURNAL OF PHYSICAL CHEMISTRY B · JULY 2007

Impact Factor: 3.3 · DOI: 10.1021/jp068692m · Source: PubMed

12 AUTHORS, INCLUDING:

Tim Albrecht
Imperial College London
65 PUBLICATIONS **1,256** CITATIONS
SEE PROFILE

Simon Higgins
University of Liverpool
154 PUBLICATIONS **3,585** CITATIONS
SEE PROFILE

Donald Bethell
University of Liverpool
260 PUBLICATIONS **11,963** CITATIONS
SEE PROFILE

Qijin Chi
Technical University of Denmark
100 PUBLICATIONS **2,305** CITATIONS
SEE PROFILE

Single-Molecule Conductance of Redox Molecules in Electrochemical Scanning Tunneling Microscopy†

W. Haiss,‡ T. Albrecht,§ H. van Zalinge,‡ S. J. Higgins,‡ D. Bethell,‡ H. Höbenreich,‡ D. J. Schiffrin,‡ R. J. Nichols,‡ A. M. Kuznetsov,|| J. Zhang,§ Q. Chi,§ and J. Ulstrup*,§

Centre for Nanoscale Science, Chemistry Department, University of Liverpool, Liverpool L69 7ZD, United Kingdom, Department of Chemistry and Nano·DTU, Technical University of Denmark, Building 207, DK-2800 Lyngby, Denmark, and The A. N. Frumkin Institute of Physical Chemistry and Electrochemistry, Russian Academy of Sciences, Leninskij Prospect 31, 119071 Moscow, Russia

Received: December 18, 2006; In Final Form: February 26, 2007

Experimental data and theoretical notions are presented for 6-[1′-(6-mercapto-hexyl)-[4,4′]bipyridinium]-hexane-1-thiol iodide (6V6) "wired" between a gold electrode surface and tip in an in situ scanning tunneling microscopy configuration. The viologen group can be used to "gate" charge transport across the molecular bridge through control of the electrochemical potential and consequently the redox state of the viologen moiety. This gating is theoretically considered within the framework of superexchange and coherent two-step notions for charge transport. It is shown here that the absence of a maximum in the $I_{tunneling}$ versus electrode potential relationship can be fitted by a "soft" gating concept. This arises from large configurational fluctuations of the molecular bridge linked to the gold contacts by flexible chains. This view is incorporated in a formalism that is well-suited for data analysis and reproduces in all important respects the 6V6 data for physically sound values of the appropriate parameters. This study demonstrates that fluctuations of isolated configurationally "soft" molecules can dominate charge transport patterns and that theoretical frameworks for compact monolayers may not be directly applied under such circumstances.

1. Introduction

There have been rapid developments of techniques and devices in which electronic transport of molecular wires and nanostructures can be addressed. In recent years it has even become possible to contact individual molecules and characterize their electrical behavior. Using the techniques of scanning tunneling microscopy (STM), conducting atomic force microscopy (c-AFM), or break junctions, single-molecular wires have been tethered between metal electrodes.[1−9] Such experiments open new possibilities for establishing mechanisms of electron transport in both organic molecules and transition metal complexes, clearly with perspectives in both fundamental single-molecule science and single-molecule technology.

A crucial contemporary question is how charge transport across single molecules can be controlled. Electrochemistry has recently been shown to provide an elegant approach to reversibly controlling charge transport across single molecules and nanoscale structures.[8−15] Electrochemical means could be employed to control accessible electronic redox levels and in doing so add novel features such as on−off switching, negative differential resistance, rectification, and other single-molecule characteristics. These features are associated with the redox levels and are not encountered in tunneling behavior of non-redox molecules where the highest occupied and lowest unoccupied orbitals (HOMO and LUMO) are strongly off-resonance with the Fermi levels of the enclosing electrodes. In this way electrochemical surface science has enabled the transfer of single-molecule conductance notions from vacuum to aqueous electrolyte.

Electrochemical gating in the in situ STM mode is achieved through a four-electrode electrochemical configuration in which the reference electrode or the counter electrode, controlled through the reference electrode, acts as a "gate" for the tunneling process. The other two electrodes, i.e., the STM tip and the substrate surface, act as contacts for the molecular wire and can be thought of as the source and drain of a single-molecule device. This is illustrated in Figure 1 for a viologen molecular wire. The redox state of the viologen group within a molecular wire tethered between two contacts in the electrochemical environment is controlled by the reference, i.e., the "gating" electrode, also immersed in the electrolyte. In contrast to STM in ultrahigh vacuum (UHV) or air (ex situ STM), a reference electrode common to the substrate and tip in the in situ STM configuration further offers both current−overpotential and current−bias voltage relations. These are analogous to current−gate and current−bias voltage relations reported for single-molecule transistors in the UHV environment.[16,17] Following reports that electrochemical approaches could be pursued to gate charge transport across single viologen molecular wires,[8] there have been studies of electrochemical gating of molecular wires, including electrode potential switching of, for example, perylene tetracarboxylic diimide[13] and hepta-aniline conductance.[14] These studies have utilized an in situ STM configuration in which the redox-active molecular wires are chemically attached between a gold substrate and the STM tip. Such behavior has also been apparent in both in situ STM and scanning tunneling spectroscopy (STS) of transition metal complexes. For instance, the electrochemical potential was used to control electron tunneling

† Part of the special issue "Norman Sutin Festschrift".

* Author to whom correspondence should be addressed. E-mail: ju@kemi.du.uk.

‡ University of Liverpool.

§ Technical University of Denmark.

|| Russian Academy of Sciences.

10.1021/jp068692m CCC: $37.00
Published on Web 05/12/2007

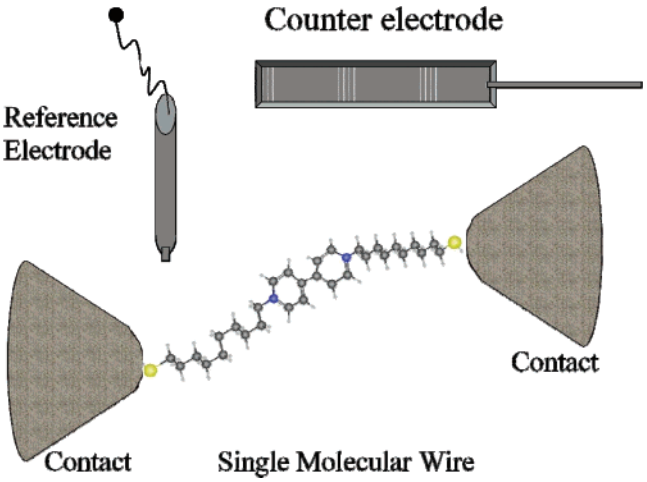

Figure 1. Redox gating of a single-molecular wire in an electrochemical setup.

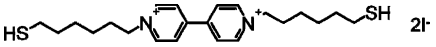

Figure 2. Structure of the redox-active molecular wire 6-[1′-(6-mercapto-hexyl)-[4,4′]bipyridinium]-hexane-1-thiol iodide, abbreviated as 6V6.

through iron protoporphyrin IX.[18] Furthermore, a comprehensive comparative study of a class of Os and Co complexes showed both electrochemical control of the in situ STM currents and consistent patterns in the overpotential, bias voltage, and equilibrium redox potentials of the target molecules.[15,19] These patterns could, finally, be compared with theoretical frameworks developed previously for in situ STM processes of redox molecules.[20−23]

In this report we provide experimental data alongside theoretical analyses that clearly demonstrate electrochemical "gating" of redox molecular wires based on viologen linked via hexane-1-thiol groups to an enclosing in situ STM substrate and tip, the potentials of which are controlled relative to a common reference electrode. The structure of 6-[1′-(6-mercapto-hexyl)-[4,4′]bipyridinium]-hexane-1-thiol iodide is shown in Figure 2, and the syntheses of this and related molecules have been described previously.[10,11,24,25] This compound is abbreviated to 6V6, where the numerals denote the number of methylene groups between the viologen N and the terminal S. This molecule was chosen for several reasons. The thiol groups at both ends constitute anchoring points to the gold surface and the STM tip. The redox-active viologen (V) group is symmetrically placed between defined molecular tunneling bridges (the two polymethylene chains) at either end. The viologen molecules are highly stable in the redox states addressed, and the viologen group (V) has readily accessible energy levels for electrochemical gating.

The current−overpotential relation (equivalent to the current−gate voltage relation in single-molecule transistors) for 6V6 shows a significant rise as the $V^{2+/+}$ equilibrium potential is approached. However, in contrast to both iron protoporphyrin IX[18] and the Os complexes,[15,19] the current does not show a maximum. The overpotential range over which the significant rise is observed is also much wider than those for the transition metal complexes. These observations are set in context through theoretical frameworks for electrochemically gated electron transport across single molecules, which include both sequential two-step and superexchange notions. A particular difference from the data for the transition metal complexes is that the latter involved ordered or dense monolayers of structurally rigid molecules, whereas the present data involve isolated, configurationally "soft" molecules. Fluctuating configurational effects can therefore be much more important. This effect can be expected to invoke significant inhomogeneous broadening effects on the viologen-based molecule(s) that are absent in the tunneling patterns for densely packed monolayers such as the transition metal complexes.

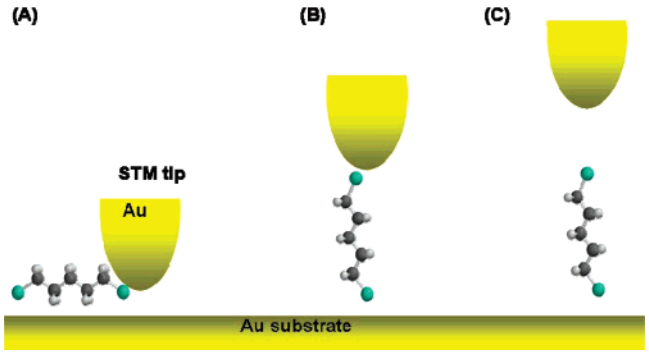

Figure 3. STM technique (called the "*I*(*s*) method") of forming molecular wires between a Au tip and a substrate for single-molecule electrical property measurement.

2. Experimental Section

Electrochemistry. The redox electrochemistry of self-assembled monolayers of 6V6 was studied by cyclic voltammetry (CV) using an AutoLabPGSTAT20 (Eco Chemie, The Netherlands) computer-controlled instrument. For the voltammetric measurements a glass cell with a Pt gauze counter electrode and a saturated Calomel reference electrode (SCE) has been used. A Au(111) single-crystal electrode was employed as the working electrode with a surface area of 1.13 cm^2. This was flame-annealed prior to the experiment, and solutions were degassed with argon.

Single-Molecule Conductance Measurements on 6V6. Single-molecule conductance measurements were performed with a Pico2000 system using Picoscan 4.19 software (Molecular Imaging Corporation). These measurements were carried out in 0.1 M phosphate buffer solution at pH 7 (K_2HPO_4/K_3PO_4 in water) in a Teflon STM cell with gold-on-glass samples, a gold counter electrode, and a quasi-reference electrode wire. Electrode potentials were converted to the SCE scale. The formation of molecular wires was performed with gold wire STM tips to facilitate thiol attachment to the tip. The thiol attachment between the gold surface (flame-annealed gold-on-glass samples with Au(111) terrace structures) and the tip was achieved with the so-called *I*(*s*) method.[8] The *I*(*s*) method of forming molecular wires between a gold STM tip and a substrate is illustrated in Figure 3. Briefly, a gold STM tip is brought into close proximity to a gold substrate, avoiding mechanical contact. The gold surface contains a low coverage of the target molecule with thiol groups at both ends. These serve the purpose of ensuring appropriate chemical and, hence, electrical contact between both ends of the molecule to the tip and surface, respectively. After positioning the tip, the feedback loop of the STM is switched off, and the tunneling current is measured as the tip is retracted from the surface. The complete current−bias voltage response can also be recorded by retracting the tip in a stepwise manner and recording current−bias voltage ($I-V_{bias}$) sweeps at each distance step.

In the case of temperature dependence measurements for nonanedithiol an alternative method of determining single-molecule conductance called the "*I*(*t*) method" was employed.[7]

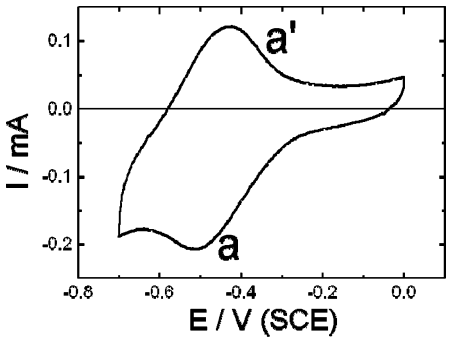

Figure 4. Cyclic voltammogram of 6V6 on Au(111). Peak a corresponds to the one-electron reduction of the bipyridinium redox center (V^{2+}) to the radical anion ($V^{+\bullet}$), i.e., $V^{2+} + e^- \rightarrow V^{+\bullet}$, while peak a′ corresponds to the reverse process ($V^{+\bullet} - e^- \rightarrow V^{2+}$).

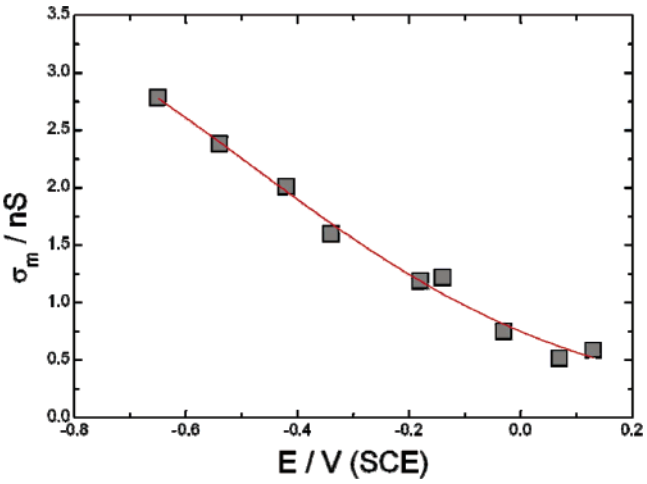

Figure 5. Measurements of the single-molecule conductance of 6V6 molecular wires under electrochemical control in 0.1 M phosphate buffer solution. The electrode potential dependence of the conductance at a constant tip−sample bias ($U_T = 0.2$ V) of a single 6V6 molecule is shown. The potential (vs SCE) on the *x*-axis of the experiment of Figure 5 is the potential average between the tip and the sample. For example, a tip voltage of −200 mV (vs substrate) at a potential of −400 mV (substrate vs SCE) gives a potential of −500 mV vs SCE. The line is only a guide for the eye.

This method involves holding the Au STM tip at a given distance above the substrate while monitoring current jumps as molecular wires bridge the tip and substrate gap and subsequently break. It has previously been shown that both the *I*(*s*) and the *I*(*t*) method result in the same single-molecule conductance for alkanedithiols.[7]

3. Experimental Results

Figure 4 shows a cyclic voltammogram for a self-assembled monolayer (SAM) of 6V6 adsorbed on Au(111). The voltammogram shows reduction/reoxidation peaks between −0.45 and −0.5 V (SCE) corresponding to one-electron redox switching of the bipyridinium redox center ($V^{2+} + e^- \Longrightarrow V^{+\bullet}$).[25,26] The corresponding single-molecular conductance data for 6V6 on the flame-annealed gold-on-glass samples with Au(111) terrace structures are shown in Figure 5, after immersion in 5×10^{-5} M 6V6 solution in methanol for 100 s. After adsorption of 6V6, the samples were washed in ethanol and blown dry with nitrogen. The electrochemical potential dependence of the single-molecule conductance of 6V6 was recorded at a constant tip−sample bias ($U_T = 0.2$ V). At 0.1 V (SCE) the viologen is in the fully oxidized state with a single-molecule conductance of 0.5 nS, while a conductance of 2.8 nS is recorded at −0.7 V,

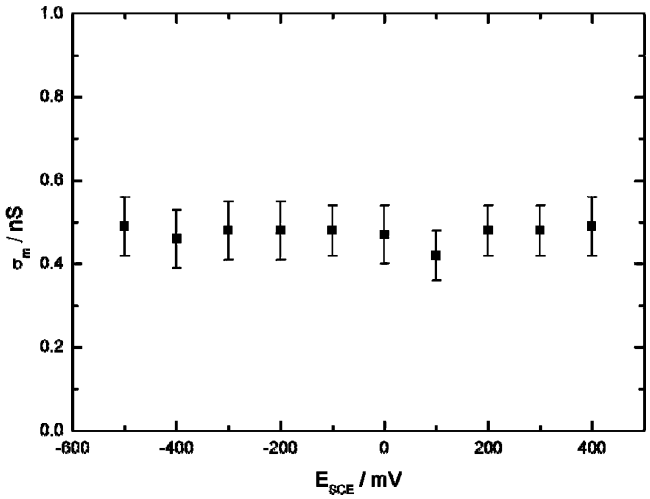

Figure 6. Electrochemical single-molecule conductance data for nonanedithiol on Au(111) in sodium phosphate buffer, with U_T = 200 mV.

where the viologen is reduced to the cation radical form. Each data point is taken from histogram peaks of current plateau values recorded using the *I*(*s*) method as described in refs 7 and 8. The single-molecule conductance rise is apparent from approximately −0.1 V, which is close to the foot of the voltammetric peak (at −0.2 V).

Figure 5 indicates that the redox-active viologen group is involved in charge transport across the 6V6 molecular wire. This behavior demonstrates that the electrode potential can then be used to gate current flow across the molecular wire with the conductance rising from 0.5 to 2.8 nS at −0.7 V.[8] The "on−off" conductance ratio is significant, i.e., a factor of 6, but the absence of a maximum in the conductance−overpotential relation around the $V^{2+/+}$ equilibrium redox potential and the broad potential range of conductance rise prompt attention to configurational fluctuational effects and other features. Control experiments are provided by simple alkanedithiol molecular wires. Figure 6 shows single-molecule conductance data for nonanedithiol (NDT) plotted as a function of electrode potential between +400 and −600 mV (SCE). It can be readily seen that there is no potential dependence of the molecular conductance within the limits of the error bars for this alkanedithiol molecule. These data together clearly show the role of the viologen group in determining the electrochemical dependence of the single-molecule conductance of 6V6.[8] Mechanisms for charge transport across the viologen molecular wire are analyzed and theoretically framed in the following sections.

Although simple alkanedithiols such as NDT do not show electrochemical gating of the single-molecule conductance they do show thermal gating; i.e., temperature can be used to control charge transport across alkanedithiol molecular wires. Experimental data obtained by the *I*(*t*) method showing the temperature dependence of single-molecule conductance are also presented here, since the theoretical analysis of tunneling mechanisms for gated electron transfer across alkanedithiols proceeds from the influence of conformational fluctuations on off-resonance tunneling. Experimental data for the temperature dependence of the single-molecule conductance of nonanedithiol in the temperature range of 20−70 °C are presented in Figure 7[26] and show that the single-molecule conductance increases from 0.52 ± 0.09 nS at 20 °C to 2.9 ± 0.4 nS at 67 °C.[26] This increase is caused by the increased population of more folded (higher-energy) conformers of NDT as the temperature is increased.[26,27] The graph in Figure 7 has the form of a thermally activated

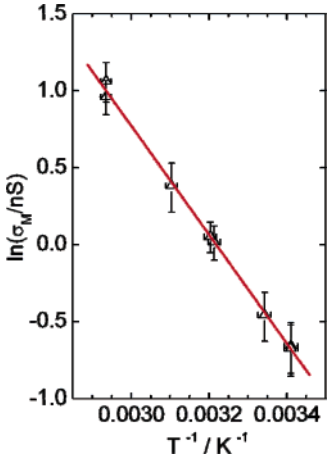

Figure 7. Logarithmic plot of the single-molecule conductance of nonanedithiol as a function of the inverse temperature (T range 20−70 °C).[26] The data were recorded using the $I(t)$ method.[7] The solid line is a linear fit with a slope of −(3533 ± 71) K (~0.3 eV). All measurements were recorded in air at $U_T = +0.2$ and $+0.4$ V; error bars represent plus or minus one standard deviation.

process, with the slope taking on the form of apparent activation energy (as discussed below). A simple tunneling model for the temperature-dependent conductance based on the conformer distribution is discussed in ref 26. In the discussion below this observation is set into a more formal framework of thermally "gated" tunneling through the alkanedithiol molecules.

4. Tunneling Mechanisms in "Gated" Off-Resonance and Resonance Electron Transfer

Two observations regarding the microscopic conductivity mechanism are particularly important. The first one concerns the effects of the nuclear dynamics and the nature of the transition as environmentally "gated" electron tunneling. The control molecule in these studies, nonanedithiol, shows no electrochemical potential dependence of single-molecule conductance (Figure 6) but does show pronounced temperature dependence (Figure 7). The observed temperature dependence cannot, however, originate in multiphonon electron transfer such as in interfacial electrochemical electron transfer or in recent cases of single-molecule conductance where low-lying redox centers (e.g., the viologen and transition metal centers) or metallic nanoparticles are involved as electronic relays. The temperature dependence offers instead a case for "gated" electron tunneling through the alkanedithiol molecules. This notion is broadly known for electron transfer and particularly for chemical and biological proton or hydrogen atom transfer processes.[28]

The notion of "gating" in the off-resonance tunneling through non-redox molecules implies that a structural nuclear equilibrium configuration of minimum energy exists, along with a distribution of other configurations of higher but thermally accessible energies. Tunneling through the minimum energy configuration is unfavorable compared to higher-energy conformations, which offer more facile tunneling in return for thermal activation. This is due to better electronic overlap or smaller energy gaps between the Fermi levels of the electrode and the HOMO or LUMO. Conformational, i.e., torsional, motion offers the most facile thermal activation. Gated electron tunneling and the observed apparent activation energy are therefore likely to involve thermally activated preorganization in these low-frequency modes. The observed activation energy thus has the status of "apparent", because in addition to thermal activation in the nuclear coordinates the structural identity (i.e., the conformer distribution) of the molecules also changes with temperature. Thermally induced conformational changes also resemble a separate "chemical reaction" step prior to electron tunneling.

The second observation relates to the purely electronic part of the tunneling process. The absence of a maximum in the single-molecular conductance versus overpotential data (Figure 5) would not be expected for a two-step process with successive reduction and reoxidation. In such a case, as the potential crosses or becomes very close to the equilibrium potential both the oxidized and the reduced forms would contribute comparably to the tunneling current. The mechanism would then most likely change into a two-step hopping mechanism giving a maximum in the tunneling current/overpotential relation such as observed elsewhere.[9,15,18] A maximum is also expected in the tunneling or superexchange mode when comparable populations of the two forms are present. In this case the observed potential dependence would be determined to a significant extent by the potential dependence of the populations of the two forms.

The absence of a maximum in the tunneling current versus overpotential relation indicates that the vacant (oxidized) redox level remains significantly off-resonance relative to the Fermi levels of the enclosing electrodes in the whole potential scan, although resonance is approached toward the negative end of the potential range. The (quantum mechanical) population of the oxidized form is thus taken to exceed significantly the population of the reduced form in the whole range and to vary insignificantly with the electrode potential. In light of this we introduce a theoretical frame for the data analysis based on the superexchange view with no population, i.e., no physical reduction, of the viologen "wire" in the STM gap configuration. We thus assume that in the STM gap configuration the effective potential remains more positive than the local equilibrium redox potential and that the oxidized form (V^{2+}) completely dominates. This disparity between the effective local potential experienced by the viologen in the STM gap configuration and the local equilibrium redox potential is introduced through the fraction of the substrate electrode solution potential to which the redox group is exposed (the term ξ, cf. below). However, the potential reaches values close enough to the equilibrium potential that the potential variation is significantly reflected in the electronic (superexchange) tunneling factor, eq 1. The small electronic energy gap is thus what causes the current rise toward the negative end of the potential range.

4.1. Tunneling through the Conducting Molecule. The following general observations illuminate theoretical frameworks for gated electron tunneling and apply to the data. We invoke the Born−Oppenheimer approximation and the notion of tunneling at fixed conformational coordinates. The latter are at first characterized by a set of collective coordinates, $\{q_k\}$, $k = 1, ..., N$. The electronic tunneling factor can be represented mathematically in several ways. Regarding the molecule as a unit with a single well-defined HOMO and LUMO the current at given $\{q_k\}$ is given by the superexchange form in eq 1[29,30]

$$i(\{q_k\}) = \frac{e}{\pi\hbar}\int_{\epsilon_F^{tip}}^{\epsilon_F^{substr}} \frac{\Delta_1(\{q_k\})\Delta_2(\{q_k\})}{[\epsilon - \epsilon_{mol}(\{q_k\})]^2 + [\Delta(\{q_k\})]^2}\,d\epsilon \qquad (1)$$

Integration is over the electronic energy levels between the Fermi levels of the substrate, ϵ_F^{substr}, and the tip, $\epsilon_F^{tip} < \epsilon_F^{substr}$; i.e., the Fermi functions are regarded as unit step functions. Also, e

is the electronic charge, and $2\pi\hbar$ is Planck's constant. The molecular interactions (broadenings of electronic energy levels) with the two metals are given in eq 2

$$\Delta_1 \approx \pi(V_s(\{q_k\}))^2\rho_S \quad \Delta_2 \approx \pi(V_t(\{q_k\}))^2\rho_T$$
$$\Delta = \Delta_1 + \Delta_2 \tag{2}$$

Here V_s and V_t are the electron exchange integrals coupling the molecular level(s) to the substrate (s) and tip (t), and ρ_S and ρ_T are the substrate and tip electronic level densities. $\epsilon_{mol}(\{q_k\})$ is the molecular energy level at given $\{q_k\}$ and overpotential and taken as

$$\epsilon_{mol}(\{q_k\}) = \epsilon_{mol}(\{q_k\};\eta) = \epsilon_a - \epsilon_F^{substr} - \sum_k \gamma_k q_k - e\xi\eta - e\varsigma V_{bias} \tag{3}$$

where ϵ_a is the molecular energy at equilibrium and $\{\gamma_k\}$ a set of coupling constants for coupling between the electronic energy levels and the conformational motion. ξ is the fraction of the substrate electrode−solution potential drop at the site of the molecular group, and ζ the fraction of the bias voltage at the molecular site; cf. above.

Equations 1−3 combined with thermal activation along the gating mode (cf. below) provide the observable tunneling current and apparent activation energy. The gating mode dependence is reflected in both energy denominators and electronic coupling (broadening). This suggests an alternative form of the electronic factor in which tunneling is more directly apparent. Instead of the overall HOMO or LUMO in eqs 1−3, group orbitals corresponding, for example, to electron or hole localization on the Au−S or $-CH_2-$ units can be introduced. Broadening then applies to the terminal groups linked to the substrate and tip, i.e., the thiolate groups, while all of the intermediate ($-CH_2-$) groups are coupled to their nearest neighbors. The resulting multilevel form is shown in eq 4[29,30]

$$i(\{q_k\}) = \frac{4e}{\pi\hbar}\Delta_{substr}\Delta_{tip}\int_{\epsilon_F^{tip}}^{\epsilon_F^{substr}}(\beta_{sub-S,j=1})^2\prod_{j=1}^{N-1}\left(\frac{\beta_{j,j+1}}{\epsilon - \epsilon_{jmol}(\{q_k\};\eta;V_{bias}) - \Gamma_j}\right)^2(\beta_{j=N,tip-S})^2\,d\epsilon \tag{4}$$

$\beta_{j,j+1}$ is the electron exchange factor for coupling between the jth and $(j+1)$th group. $\beta_{sub-S,j=1}$ is the exchange factor for coupling of the first $-CH_2-$ group to the thiol linker at the substrate, and $\beta_{j=N,tip-S}$ for coupling of the Nth $-CH_2-$ group to the thiol linker at the tip. Γ_j ($\approx \beta_{j-1,j} + \beta_{j,j+1}$) is the exchange coupling for all of the couplings in which the jth group is engaged.

We invoke the following three assumptions

$$\beta_{j,j+1} = \beta_{sub-S,j=1} = \beta_{j=N,tip-S} = \beta$$

$$\epsilon - \epsilon_{jmol}(\{q_k\};\eta;V_{bias}) = \epsilon - (\epsilon_a - \epsilon_F^{substr} - \sum_k \gamma_k q_k - e\xi_{aver}\eta - e\varsigma_{aver}V_{bias}) = \Delta E_{gap}(\epsilon;\{q_k\};\eta;V_{bias}) \tag{5}$$

$$\Gamma_j \ll \epsilon - (\epsilon_a - \epsilon_F^{substr} - \sum_k \gamma_k q_k - e\xi_{aver}\eta - e\varsigma_{aver}V_{bias}) \tag{6}$$

for all j. The subscript "aver" indicates that we have taken an average value of the effects of the overpotential and bias voltage on all of the groups. This reduces the number of parameters drastically but can be relaxed straightforwardly. All overpotential and bias voltage dependences have, moreover, been associated with the energy gaps. The assumption of constant, i.e., energy-independent, electronic coupling factors applies approximately at energies off-resonance with the Fermi energies of the enclosing electrodes but can be relaxed as warranted.[31] Equation 4 can then be converted to the form given in eq 7

$$i(\{q_k\}) = \frac{4e}{\pi\hbar}\frac{\Delta_{substr}\Delta_{tip}}{\beta^2}\int_{\epsilon_F^{tip}}^{\epsilon_F^{substr}}\left(\frac{\beta}{\Delta E_{gap}(\epsilon;\{q_k\};\eta;V_{bias})}\right)^{2N}d\epsilon = \frac{4e}{\pi\hbar}\frac{\Delta_{substr}\Delta_{tip}}{\beta^2}\int_{\epsilon_F^{tip}}^{\epsilon_F^{substr}}\times \exp\left\{-\left[\frac{2}{a}\ln\left(\frac{\Delta E_{gap}(\epsilon;\{q_k\};\eta;V_{bias})}{\beta}\right)R\right]\right\}d\epsilon \tag{7}$$

where a is the average extension of each $-CH_2-$ group and $Na = R$ is the tunneling distance along the $-(CH_2)_n-$ chain. The overpotential dependence according to eqs 3 and 5 is indicated. These equations bridge electronic conduction through the molecular structure with a tunneling form. Temperature and overpotential variation of the tunneling current emerges primarily from the energy gap dependence of these quantities, $\Delta E_{gap}(\epsilon;\{q_k\};\eta)$.

4.2. Thermal Averaging along Gating Modes. "Gating" in the conformational $-(CH_2)_n-$ chain system precedes the tunneling process, which is induced at fixed, nonequilibrium conformations. "Gating" or "fluctuational barrier preparation" has been extensively addressed in solid-state coherent and incoherent tunneling processes, in diffusion of solid-state impurities, and in chemical and biological proton and hydrogen atom transfer processes.[28] Both high-temperature thermally activated and low-temperature nuclear tunneling in the gating modes have, moreover, been addressed.[28] In the present case gating is considered in a simple approach, restricted to thermal averaging of the tunneling current over a classical Boltzmann distribution of low-frequency conformational gating coordinates. In the analysis we consider the two cases above separately, i.e., off-resonance electron tunneling through a molecule with no redox group and the case of a dominating low-lying redox group in the conductivity channel. The effects of the gating mode appear rather differently in the two cases.

4.3. Thermal Averaging along the Gating Mode in Off-Resonance Superexchange. Equation 7 is generalized to give the observed current density as

$$i(\eta;V_{bias}) = Z^{-1}\int_{-\infty}^{\infty}\prod_k dq_k \exp\left[-\frac{U(\{q_k\})}{k_BT}\right]i(\{q_k\};\eta;V_{bias})$$
$$Z = \int_{-\infty}^{\infty}\prod_k dq_k \exp\left[-\frac{U(\{q_k\})}{k_BT}\right] \tag{8}$$

where $U(\{q_k\})$ is the conformational potential energy surface and Z is the classical configurational integral. Two observations emerge. First, assuming that the bias voltage is small as by eq 9

$$|e\varsigma_{aver}V_{bias}| \ll \epsilon_a - \epsilon_F^{substr} - \sum_k \gamma_k q_k - e\xi\eta \tag{9}$$

we can replace ϵ in eqs 5, 7, and 8 by the Fermi energy of the substrate, ϵ_F^{substr}. Second, the Boltzmann factor and the tunneling current, $i(\{q_k\};\eta;V_{bias})$ in eq 7, show opposite dependences on the conformational fluctuations. The former decreases when

the $\{q_k\}$ set fluctuates from equilibrium, whereas $i(\{q_k\};\eta)$ increases due to the decreasing tunneling barrier. Equation 8 can therefore approximately be replaced by

$$i(\eta) \approx \frac{4e}{\pi\hbar}\frac{\Delta_{substr}\Delta_{tip}}{\beta^2}Z^{-1}|eV_{bias}| \times \exp\left[-\frac{2}{a}\ln\left(\frac{\Delta E_{gap}(\epsilon_F\{q_k^*(\eta;V_{bias}\};\eta;V_{bias})}{\beta}\right)\right]\{\Delta q_k^*\} \times \exp\left[-\frac{U(\{q_k^*(\eta;V_{bias})\})}{k_BT}\right] \quad (10)$$

where $\{q_k^*(\eta;V_{bias})\}$ is the value of $\{q_k\}$ where the integrand in eq 8 is maximum and $\{\Delta q_k^*\}$ the width of $\{q_k\}$ which contributes. Eq 10 shows in a simple way the origin of observed apparent activation energies in the off-resonance limit of electron tunneling through a molecule with repetitive molecular fragment units such as the alkane dithiols or molecules with units of weakly varying energy gaps and exchange integrals.

When a single group with a lower energy gap is present, eq 1 is more conveniently taken as the basis, giving

$$i(\eta) \approx \frac{e}{\pi\hbar}\frac{\Delta_{substr}\Delta_{tip}}{\beta^2}Z^{-1}\{\Delta q_k^*\}|eV_{bias}| \frac{\Delta_1(\{q_k^*(\eta;V_{bias})\})\Delta_2(\{q_k^*(\eta;V_{bias})\})}{[\epsilon_F^{substr} - \epsilon_a(\{q_k^*(\eta;V_{bias})\})]^2 + [\Delta(\{q_k^*(\eta;V_{bias})\})]^2} \times \exp\left[-\frac{U(\{q_k^*(\eta;V_{bias})\})}{k_BT}\right] \quad (11)$$

This form is convenient for the viologen-based molecules. The overpotential dependence can be significant since the energy denominator in the second line assumes small values (still within the superexchange regime) as the equilibrium potential is approached.

Equations 10 and 11 represent the current−overpotential and current−bias voltage relations of alkane dithiols and viologen-based molecules, respectively, in broad potential ranges that do not, however, reach values where the off-resonance or redox levels are physically populated. In view of recent reports of redox-induced tunneling spectroscopic features and tunneling current maxima of viologens transition metal complexes in overpotential ranges around the equilibrium potential,[9,15,18,19] it seems at first surprising that the single viologen-based molecule does not exhibit such a feature. We discuss reasons for this below. For the sake of comparison the formalism of two-step sequential electron transfer, where a redox molecular group is successively reduced and oxidized (or vice versa), is briefly summarized in the Appendix.

5. Numerical Analysis of In Situ STM of Dithiol-Viologen by Superexchange

5.1. Some Observations on the 6V6 Behavior in the In Situ STM Gap. The 6V6 monolayers show a pair of clear voltammetric peaks with a midpoint potential of −0.42 V (vs SCE) corresponding to the first electrochemical ($V^{2+} + e^- \Rightarrow V^+$) transition. The in situ STM tunneling current at constant bias voltage shows a clear rise close to this potential but no maximum such as expected from patterns for the sequential two-step in situ STM mechanism of redox molecules.[9,21,32] The tunneling current instead continues to rise until approximately −0.6 V (vs SCE). The overpotential range over which the rise is observed is also much wider than that observed, for example, for the transition metal complexes.[18,33,34] This prompts the following observations:

•The voltage drop can be closer to a steplike function with most of the potential drop confined to the Au−S contacts such as suggested by quantum chemical computations.[35,36] This would attenuate the potential correlation. Current−distance relations indicate that the linker groups are likely to be in an upright position, and structural asymmetry is therefore less likely.[8]

•Double-layer effects are expected to induce electrochemical potential asymmetry in the tunneling gap and rectification in the tunneling current−bias voltage correlations[27,37] but not to be immediate causes of the broad current−overpotential rise of 6V6. Co-adsorption of counterions and possibly water repolarization in the wide overpotential range scanned could rather induce such effects and attenuate redox-based features.

•Finally, an important difference from Fe protoporphyrin IX and the Os complexes, previously shown to display clear current−overpotential maxima with high on−off current ratios, is that these target molecules were based on rigid molecules in dense monolayers, in some cases showing extended lateral order. The same applies to 6V6 in dense ordered monolayers.[9] The present data refer to single, almost isolated, molecules conformationally much more flexible than the porphyrin and Os complexes. The 6V6 molecule is therefore much more susceptible to environmental configurational fluctuational effects than the porphyrin and Os complexes. Such effects have been shown to cause large variations in the electronic energies approaching a substantial fraction of an electronvolt.[38] The single-molecule viologen data could therefore well display a significantly congested current−overpotential pattern compared with the porphyrin and Os complexes. We shall represent the fluctuational effects by a "soft" gating mode with substantial fluctuational amplitudes, which is much more important here than for the rigid and well-ordered monolayers of Fe protoporphyrin and the Os complexes.

With these reservations we take the superexchange form represented by eq 11 as the basis for the discussion below. The significant rise around the formal bulk potential but absence of a maximum is then caused by the approach of the molecular redox level to the Fermi levels of the enclosing electrons. The wide overpotential range, over which the tunneling current rises, is associated particularly with configurational and energetic fluctuational effects, jointly represented by a soft gating mode, and further convoluted with the bias voltage.

5.2. In Situ STM and Gated Electron Tunneling through 6V6 and NDT. We provide here computations of the current−overpotential and current−bias voltage relations representative of 6V6 in the in situ STM tunneling gap. In comparison, similar computations are performed for the non-redox reference molecule, 1,9-nonanedithiol (NDT). Equation 11 is used for 6V6, and eq 10 for NDT. We convert the equations to a simpler form using the following notions:

•All energies are counted from ϵ_F^{substr}.

•The $\{q_k\}$ set is represented by a single mode of low frequency, ω.

•The coupling constants $\{\gamma_k\}$ are then also reduced to a single value γ.

•The coupling constant is recast as an apparent activation energy along the conformational coordinate, E_{Aconf}^{app}, by $\gamma = \sqrt{2E_{Aconf}^{app}\hbar\omega}$, as E_{Aconf}^{app} may be a more appealing quantity than γ.

•The "critical" q-value, q^*, in eqs 10 and 11 depends on the

overpotential η and the bias voltage V_{bias}. For numerical investigations we revert, however, to the integral q-form, eq 8.

•Energies are counted in units of k_BT.

•The potential distributions in the tunneling gap are given the simplest forms, $\xi = 1$ and $\zeta = {}^1/_2$ for 6V6. This assumption can be relaxed straightforwardly. Smaller ξ-values are needed for NDT; cf. below.

•The computational current−voltage relations are normalized to the form

$$i_{norm} = i(\eta)/\left(\frac{e}{\pi\hbar}\frac{\Delta_{substr}\Delta_{tip}}{\beta^2}Z^{-1}\right) \quad (12)$$

•The electronic broadening parameters are taken to be the same for both the substrate and the tip, i.e., $\Delta_1 \approx \Delta_2 \approx \Delta_{aver}$; cf. above.

The following forms of eqs 8−11 are then used in the numerical study:

For the 6V6 viologen molecule

$$i_{norm} = |eV_{bias}|\int_{-\infty}^{\infty} dq \frac{(\Delta_{aver})^2}{(\epsilon_a - \sqrt{2E_{Aconf}^{app}\hbar\omega}\, q - e\eta - ({}^1/_2)eV_{bias})^2 + (2\Delta_{aver})^2} \times \exp(-bq^2) \quad (13)$$

For the 1,9-nonanedithiol reference molecule

$$i_{norm} = |eV_{bias}|\int_{-\infty}^{\infty} dq \exp\left\{-\left[\ln\left(\left(\frac{\epsilon_a - \sqrt{2E_{Aconf}^{app}\hbar\omega}q - \xi_{aver}e\eta - ({}^1/_2)eV_{bias}}{\beta}\right)\frac{R}{a}\right)\right]\right\} \times \exp(-bq^2) \quad (14)$$

Suitable parameter values in the numerical computation are:

• ϵ_a is taken as 1−3 eV for NDT and 0.5 eV for 6V6, i.e., $40-120k_BT$ and $20k_BT$, respectively.

•The average electronic broadenings are assigned values in the range of $\Delta_{aver} = 1-5k_BT$.

•The electronic−vibrational coupling, $\gamma = \sqrt{2E_{Aconf}^{app}\hbar\omega}$, is given values in the range of 1−10. In the harmonic approximation the conformational parameter $b = {}^1/_2\, \eta\omega/k_BT$. As conformationally "soft" dynamics are in focus, b is given values in the range of 0.01−1.

•The quantity ξ_{aver} in front of $e\eta$ in eq 14 represents the incomplete double-layer screening of the superexchanging groups, say, $-CH_2-$ groups, in the NDT bridge. ξ_{aver} depends on the distance of the groups from the electrode surface and varies from a value between zero close to the surface to unity at distances exceeding the Debye length (∼10 Å). An average value of $\xi_{aver} \approx {}^1/_2$ was first chosen, but smaller values were needed to reproduce the almost complete overpotential independence of the conductance of NDT. Distance variation can be invoked by using the more general form in eq 4. ξ_{aver} can be replaced by unity in eq 13 as the viologen group is sufficiently remote from the electrode surface.

Figure 8 shows plots of the normalized gated superexchange tunneling current versus the overpotential, eq 13, representative of 6V6. The overpotential range is 0.5 V. A significant tunneling current variation, of the same order as observed, i.e., a factor of 6 or so, is seen for a "soft" gating mode, representative of conformational fluctuations. Unambiguous values of the parameters $\hbar\omega$ and γ cannot, however, be determined completely independently. $\hbar\omega$ values around 15−20 cm^{-1} ($b = 0.03-0.05$) and γ values in the range of $\gamma = (1-2) \times k_BT$ appear to be the best compromise between current−overpotential correlations, approaching most closely the correlation observed experimentally and reasonable values of the apparent activation energy along the gating mode, E_{Aconf}^{app}. $\hbar\omega = 20$ cm^{-1} ($b = 0.05$) and $\gamma = 1.0 \times k_BT$ give, for example, $E_{Aconf}^{app} \approx 0.13$ eV, while $\hbar\omega = 15$ cm^{-1} ($b = 0.0375$) and $\gamma = 1.6k_BT$ give $E_{Aconf}^{app} = 0.42$ eV. Both of these combinations accord well with the data. In comparison, $E_{Aconf}^{app} \approx 0.3$ eV for NDT of a similar length. Larger values of γ and $\hbar\omega$ give either current−overpotential shapes and current enhancement factors in significantly discord with the experimental data or unphysically large values of E_{Aconf}^{app}. The view and formalism of superexchange through the low-lying $V^{2+/+}$ state thus seem to accord satisfactorily with the tunneling conductivity data for 6V6.

The data for NDT conductance, Figures 9 and 10, are harder to rationalize with eq 14. The apparent activation energy is considerable, i.e., ∼0.3 eV (gas-phase value); cf. above; i.e., $\gamma = 0.015-0.02$ eV for $\hbar\omega = 10-20$ cm^{-1}. This would give a finite overpotential dependence of the conductance. A larger vibrational gating frequency would attenuate the overpotential

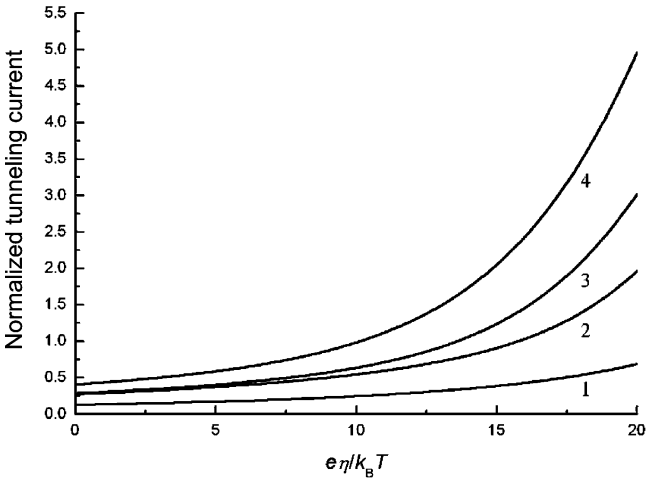

Figure 8. Dependence of the normalized tunneling current (eq 13) on the overpotential. The width of the electronic energy level $\Delta = 0.025$ eV; $\gamma = 1$, $b = 0.05$ (curve 1); $\gamma = 1.6$, $b = 0.00375$ (curve 2); $\gamma = 2$, $b = 0.00375$ (curve 3); $\gamma = 1.6$, $b = 0.002$ (curve 4).

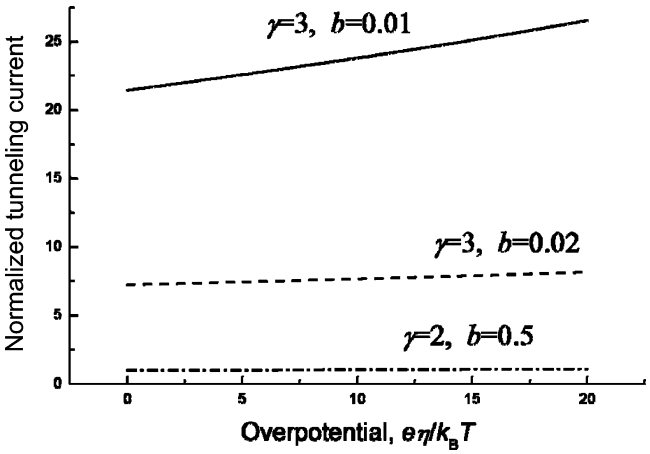

Figure 9. Normalized tunneling current vs the overpotential, eq 14, representative of NDT. Energies are given in units of k_BT. $\epsilon_a = 120$; $\beta = 8$; $\xi_{aver} = 0.1$; $R/a = 6$. γ- and b-values are indicated in the figure. The lower two curves correspond to the experimental data in Figure 6. Larger values of ξ_{aver} give significant overpotential dependence of the tunneling current.

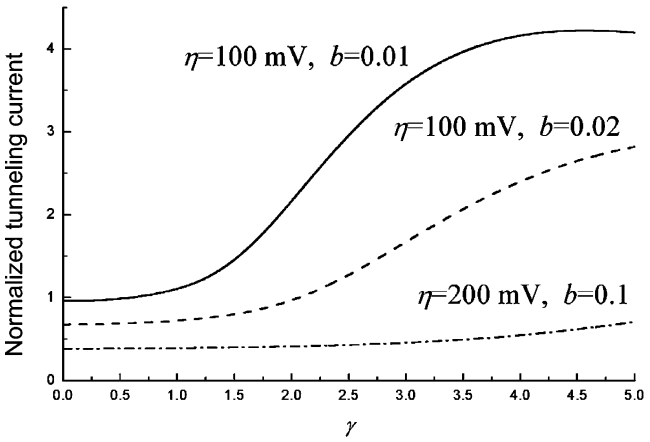

Figure 10. Effect of the coupling constant $\gamma = \sqrt{2E_{A,conf}^{app}\hbar\omega}$ on the gating mode, eq 13, representative of 6V6. Energies are given in units of k_BT. $\epsilon_a = 40 \times k_BT$. *b*- and η-values are indicated in the figure.

dependence but even values of ϵ_a up to 3 eV above the Fermi level of the substrate electrode and vibrational frequencies at the boundary of classical behavior, 200−400 cm^{-1}, corresponding to $\gamma = 0.05-0.06$ eV or $(2-3) \times k_BT$, leave a variation of the conductance by a factor of 2 or so over the potential range use. Only if the double-layer screening factor, ξ_{aver}, takes small values, say, 0.1−0.2, does the overpotential dependence reduce to almost insignificance. This is shown in Figure 9 based on eq 14 and representative values of the other parameters. Other factors thus seem to cancel the gating effect to give the observed complete independence of the overpotential shown in Figure 6.

Figure 10 illustrates the effect of the electronic−vibrational coupling on the gating mode, eq 13. This effect is notable for soft modes but weaker than for the overpotential dependence.

Conclusions

There is now a growing body of experimental evidence that demonstrates that electrochemistry can be used to control the conductance of redox-active molecular wires tethered between metallic contacts. The data for 6V6 wires containing the redox-active viologen moiety reported here show the single-molecule conductance dependence of electrode potential recorded at constant bias in an in situ STM configuration with gold contacts. A clear 6-fold rise in conductance on adjusting the electrode potential from values where the viologen moiety is oxidized (V^{2+}) to values where it is reduced ($V^{+\bullet}$) is seen. The rise evolves over a 0.5−0.6 V overpotential variation.

The current−overpotential pattern for 6V6 differs from those of other recently reported redox systems. The pattern is also quite distinct from those of similar-sized non-redox molecular contacts, here represented by NDT, the conductance of which is completely independent of the overpotential. This points to a clear role of the $V^{2+/+\bullet}$ redox group. However, the data for 6V6 do not display the maximum in the current−overpotential relation expected for sequential two-step reduction−oxidation cycles of the viologen group based on theoretical notions[21,32] and supported particularly by data for Fe protoporphyrin IX,[18] Os complexes,[15,19] and mono-viologens.[9]

The data reported presently, however, represent a redox molecular system with important differences also from those for which strong current enhancement and a "spectroscopic" current−overpotential feature have been reported. The most important difference is that the reported spectroscopic current−overpotential features appear for systems where a target molecule is either structurally rigid or has been incorporated in a two-dimensional ordered monolayer or in other ways adsorbed in structurally well-defined configurations.[39] The data presently reported refer both to single, in all respects isolated molecules, and to a target molecule with structurally flexible links to the enclosing electrode surfaces. These differences call for obvious modifications of both common superexchange views of molecular conductance and views of sequential two-step electron transfer through well-defined, structurally rigid molecular entities.

The data for 6V6 offer no immediate evidence for two-step electron transfer with full intermediate state vibrational relaxation. The single-molecule conductance displays, however, a significantly stronger overpotential dependence than expected and observed for single-molecule conductance of the non-redox molecule nonanedithiol. We have therefore taken the superexchange view as a theoretical basis for the data interpretation. Superexchange in situ STM processes can also display strong overpotential dependence if the mechanism is dominated by a single electronic (HOMO or LUMO) level of significantly lower energy than for other levels in the linker or solvent environment. Such a level is exactly what is represented by the redox level of the $V^{2+/+\bullet}$ group.

We have further invoked the notion of gated (but still by superexchange) conductance. This concept was introduced early in molecular charge transfer theory.[28] It follows naturally from the view that the molecular configuration most facile for electron transfer (tunneling) is not the equilibrium (fluctuational) configuration where the tunneling distance may be prohibitively long. A certain, nonequilibrium preorganization in the molecular and environmental structure instead prepares a configuration for shorter, more facile electron transfer. Preorganization is more important for the "softer" preorganizational nuclear mode, and focus on the soft, say, torsional linker group modes in the alkanedithiol-based linking units of our target system(s), accords with such a view. Soft mode gating of superexchange-based electron transfer is obviously much more important for redox than for non-redox molecules. The crucial energy level variation with overpotential, bias voltage, and conformational fluctuations is thus much stronger in the former case than in the latter due to the smaller energy denominator in the tunneling current expressions; cf. eqs 7, 13, and 14.

The theoretical analysis based on these views broadly accords with the experimental data, and the formalism offered reproduces in all important respects the 6V6 data for physically sound values of the parameters. Soft mode vibrational frequencies in the range of 10−20 cm^{-1} and couplings of $\gamma = 25-40$ meV constitute the best compromise between the current−overpotential correlation and "reasonable" values of the apparent gating activation energy in the gating mode, E_{Aconf}^{app}. The latter quantity takes quite large values, say, around 0.5 eV, which is, however, still close to apparent activation energies for gating-induced tunneling in comparable non-redox molecules, cf. Figure 7 and ref 26. Satisfactory fits cannot be obtained, neither in a sequential two-step mechanism nor in a superexchange mechanism through high-energy intermediate electronic states. Together with previous analysis,[26,40] this demonstrates the importance of conformational dynamics in charge transport across single molecules.

Appendix

Sequential Two-Step Electron Transfer of In Situ STM Processes of Redox Molecules. For the sake of completion we compare briefly the superexchange modes, eqs 10 and 11, with the sequential two-step electron-transfer mechanism of in situ

STM of redox molecules.[21,32] This mechanism is important for redox levels, with full relaxation between the steps.

The tunneling current, $i(\eta,V_{bias})$ is recast in terms of interfacial electrochemical single-electron-transfer rate constants, i.e.,

$$i_{tunn}(\eta,V_{bias}) = 2en\frac{k^{o/r}k^{r/o}}{k^{o/r}+k^{r/o}} \quad \text{(A1)}$$

$k^{o/r}$ and $k^{r/o}$ are the rate constants for reduction and oxidation of the redox molecule, respectively, at the substrate and tip. n is the number of electrons transferred coherently while the redox level relaxes through the energy window between the two Fermi levels. Both electron and hole transfer in either direction between substrate and tip are represented by this form. The rate constants follow patterns from interfacial electrochemical electron transfer, i.e.,

$$k^{o/r} = \kappa_{eff}^{ox}\frac{\omega_{eff}}{2\pi}\exp\left[-\frac{(E_r - e\xi\eta - e\varsigma V_{bias})^2}{4E_r k_B T}\right]$$

$$\kappa_{eff}^{ox} \approx \pi\kappa_{ox}\rho k_B T$$

$$k^{r/o} = \kappa_{eff}^{red}\frac{\omega_{eff}}{2\pi}\exp\left\{-\frac{[E_r + e\xi\eta - (1-\varsigma)eV_{bias}]}{4E_r k_B T}\right\}$$

$$\kappa_{eff}^{red} \approx \pi\kappa_{red}\rho k_B T \quad \text{(A2)}$$

where E_r is the local and environmental reorganization free energy, and ω_{eff} the effective vibrational frequency of all the nuclear modes reorganized. κ_{ox} and κ_{red} are the electronic transmission coefficients for reduction and oxidation of the molecular redox group, respectively, involving individual metallic electronic energy levels, while κ_{eff}^{ox} and κ_{eff}^{red} are corresponding effective transmission coefficients. The latter take into account that a large number of electronic levels, of the order $\pi\rho k_B T \gg 1$ contribute to each interfacial electron-transfer step.

Two different patterns arise depending on the weak- (diabatic) and strong-coupling (adiabatic) limit of redox molecule−electrode interaction. In the former case κ_{eff}^{ox}, $\kappa_{eff}^{red} \ll 1$. Only a single electron, $n = 1$ is then transferred in the in situ STM process. However, in the adiabatic limit of strong redox molecule−electrode interaction κ_{eff}^{ox}, $\kappa_{eff}^{red} \to 1$, and a large number, of the order $n \approx (1/2)\kappa_{el}\rho|eV_{bias}| \gg 1$, where $\kappa_{el} \approx \kappa_{ox} \approx \kappa_{red}$ and ρ is the metallic electron density (taken as the same for both electrodes), is transferred. Much higher tunneling currents can thus be expected. The implications of this can be appreciated by the following considerations.

The tunneling current in eq A1 has a maximum in the current−overpotential relation close to the equilibrium potential; cf. below. For an electronically symmetric contact, $\kappa_{ox} = \kappa_{red}$ the following form applies[22] for small overpotentials ($|e\eta| \ll E_r$) and bias voltages $|eV_{bias}| < E_r$

$$i(\eta,V_{bias}) = e(eV_{bias})\kappa_{el}\rho\frac{\omega_{eff}}{2\pi}\exp\left(-\frac{E_r - eV_{bias}}{4k_B T}\right)\left\{\cosh\left[\frac{((1/2)-\varsigma)eV_{bias} - \xi\eta}{2k_B T}\right]\right\}^{-1} \quad \text{(A3)}$$

with a maximum at

$$\eta = \eta_{max} = \frac{1}{\xi}\left(\frac{1}{2} - \varsigma\right)V_{bias} \quad \text{(A4)}$$

$\eta_{max} = 0$, i.e., at the equilibrium redox potential in symmetric contacts, $\zeta = 0.5$. η_{max} can be shifted either by geometric ($\zeta \to 1$ or 0) or electronic asymmetry ($\kappa_{eff}^{ox} \neq \kappa_{eff}^{ox}$) in the tunneling gap.

An implication of this is that the maximum in the tunneling current is at an electrochemical potential for which an activation free energy of the order $1/4\ E_r \approx 0.05-0.1$ eV remains, giving a one or 2 orders of magnitude lower value of the interfacial electrochemical electron-transfer rate constant than the maximum possible value, $\kappa_{eff}^{el}(\omega_{eff}/2\pi)$. In the diabatic limit $n = 1$ in eqs A1 and A3. Since $\omega_{eff}/2\pi \approx 10^{11}-10^{12}$ s^{-1}, two-step tunneling currents would then escape detection if $\kappa_{el}\rho(eV_{bias})$ ($\ll 1$) is too small. However, $n \approx (1/2)\kappa_{el}\rho|eV_{bias}| \gg 1$ (up to several orders of magnitude) in eq A3 in the adiabatic limit, and two-step tunneling could be detected even if a significant activation free energy remains. The adiabatic or weakly diabatic limits are therefore crucial in experimental approaches to two-step electron transfer in situ STM mechanisms.

The following observations apply to the issue of gating for two-step in situ STM processes:

- Each of the rate constants in eq A2 is in principle "gated" in a way analogous to the superexchange mechanisms represented by eqs 10 and 11. Fluctuations along the gating mode(s) appear as an additional activation (free) energy, $U(\{q_k^*\})$; cf. eqs 10 and 11.
- Gating activation (free) energy, however, appears along with the reorganization free energy term, E_r, which is absent in gated superexchange. The origin of the temperature dependence of the tunneling current or conductance is thus significantly different for superexchange and two-step sequential electron transfer, but experimental distinction between the two contributions in the two-step mechanism is hardly feasible. The two mechanisms cannot therefore be distinguished merely from the temperature dependence, but the overpotential and bias voltage dependence of the tunneling current is different and in principle mechanistically diagnostic.

Acknowledgment. Financial assistance from Engineering and Physical Sciences Research Council under Grant No. EP/C00678X/1 (Mechanisms of Single-Molecule Conductance) is acknowledged by the Liverpool group. Financial support from The Leverhulme Foundation, Contract No. F/070058/T from the Russian Foundation for Basic Research, Project No. 06-03-32193, to A.M.K., and from the Danish National Research Council for Technology and Production Sciences, Contract No. 26-00-0034, to J.U., Q.C., and J.Z. is gratefully acknowledged.

References and Notes

(1) Reed, M. A.; Zhou, C.; Muller, C. J.; Burgin, T. P.; Tour, J. M. *Science* **1997**, *278*, 252.
(2) Kergueris, C.; Bourgoin, J. P.; Palacin, S.; Esteve, D.; Urbina, C.; Magoga, M.; Joachim, C. *Phys. Rev. B* **1999**, *59*, 12505.
(3) Reichert, J.; Weber, H. B.; Mayor, M.; von Lohneysen, H. *Appl. Phys. Lett.* **2003**, *82*, 4137.
(4) Reichert, J.; Ochs, R.; Beckmann, D.; Weber, H. B.; Mayor, M.; von Lohneysen, H. *Phys. Rev. Lett.* **2002**, *88*, 176804.
(5) Xu, B. Q.; Tao, N. J. J. *Science* **2003**, *301*, 1221.
(6) Cui, X. D.; Primak, A.; Zarate, X.; Tomfohr, J.; Sankey, O. F.; Moore, A. L.; Moore, T. A.; Gust, D.; Harris, G.; Lindsay, S. M. *Science* **2001**, *294*, 571.
(7) Haiss, W.; Nichols, R. J.; van Zalinge, H.; Higgins, S. J.; Bethell, D.; Schiffrin, D. J. *Phys. Chem. Chem. Phys.* **2004**, *6*, 4330.
(8) Haiss, W.; van Zalinge, H.; Higgins, S. J.; Bethell, D.; Hobenreich, H.; Schiffrin, D. J.; Nichols, R. J. *J. Am. Chem. Soc.* **2003**, *125*, 15294.
(9) Li, Z.; Han, B.; Meszaros, G.; Pobelov, I.; Wandlowski, T.; Blaszczyk, A.; Mayor, M. *Faraday Discuss.* **2006**, *131*, 121.
(10) Gittins, D. I.; Bethell, D.; Schiffrin, D. J.; Nichols, R. J. *Nature* **2000**, *408*, 67.
(11) Haiss, W.; Nichols, R. J.; Higgins, S. J.; Bethell, D.; Hobenreich, H.; Schiffrin, D. J. *Faraday Discuss.* **2004**, *125*, 179.

(12) Haiss, W.; van Zalinge, H.; Hobenreich, H.; Bethell, D.; Schiffrin, D. J.; Higgins, S. J.; Nichols, R. J. *Langmuir* **2004**, *20*, 7694.
(13) Xu, B. Q.; Xiao, X. Y.; Yang, X. M.; Zang, L.; Tao, N. J. *J. Am. Chem. Soc.* **2005**, *127*, 2386.
(14) Chen, F.; He, J.; Nuckolls, C.; Roberts, T.; Klare, J. E.; Lindsay, S. *Nano Lett.* **2005**, *5*, 503.
(15) Albrecht, T.; Guckian, A.; Ulstrup, J.; Vos, J. G. *IEEE Trans. Nanotechnol.* **2005**, *4*, 430.
(16) Park, H.; Park, J.; Lim, A. K. L.; Anderson, E. H.; Alivisatos, A. P.; McEuen, P. L. *Nature* **2000**, *407*, 57.
(17) Liang, W. J.; Shores, M. P.; Bockrath, M.; Long, J. R.; Park, H. *Nature* **2002**, *417*, 725.
(18) Tao, N. J. *Phys. Rev. Lett.* **1996**, *76*, 4066.
(19) Albrecht, T.; Guckian, A.; Ulstrup, J.; Vos, J. G. *Nano Lett.* **2005**, *5*, 1451.
(20) Kuznetsov, A. M.; Ulstrup, J. *J. Phys. Chem. A* **2000**, *104*, 11531.
(21) Kuznetsov, A. M.; Ulstrup, J. *Probe Microsc.* **2001**, *2*, 187.
(22) Zhang, J.; Chi, Q.; Kuznetsov, A. M.; Hansen, A. G.; Wackerbarth, H.; Christensen, H. E. M.; Andersen, J. E. T.; Ulstrup, J. *J. Phys. Chem. B* **2002**, *106*, 1131.
(23) Zhang, J. D.; Chi, Q. J.; Albrecht, T.; Kuznetsov, A. M.; Grubb, M.; Hansen, A. G.; Wackerbarth, H.; Welinder, A. C.; Ulstrup, J. *Electrochim. Acta* **2005**, *50*, 3143.
(24) Gittins, D. I.; Bethell, D.; Nichols, R. J.; Schiffrin, D. J. *Adv. Mater.* **1999**, *11*, 737.
(25) Gittins, D. I.; Bethell, D.; Nichols, R. J.; Schiffrin, D. J. *J. Mater. Chem.* **2000**, *10*, 79.
(26) Haiss, W.; van Zalinge, H.; Bethell, D.; Ulstrup, J.; Schiffrin, D. J.; Nichols, R. J. *Faraday Discuss.* **2006**, *131*, 253.
(27) Kornyshev, A. A.; Kuznetsov, A. M. *Chem. Phys.* **2006**, *324*, 276.
(28) Kuznetsov, A. M.; Ulstrup, J. *Electron Transfer in Chemistry and Biology: An Introduction to the Theory*; Wiley Series in Theoretical Chemistry; Wiley: Chichester, U. K., 1999.
(29) Datta, S. *Electronic Transport in Mesoscopic Systems*; Cambridge University Press; Cambridge, U. K., 1995.
(30) Kuznetsov, A. M.; Ulstrup, J. *J. Electroanal. Chem.* **2004**, *564*, 209.
(31) Kuznetsov, A.M.; Schmickler, W. *Chem. Phys. Lett.* **2000**, *327*, 314.
(32) (a) Kuznetsov, A. M.; Ulstrup, J. *J. Phys. Chem. A* **2000**, *104*, 11531. (b) Kuznetsov, A. M.; Ulstrup, J. *J. Phys. Chem. A* **2001**, *105*, 7494.
(33) Albrecht, T.; Moth-Poulsen, K.; Christensen, J. B.; Guckian, A.; Bjornholm, T.; Vos, J. G.; Ulstrup, J. *Faraday Discuss.* **2006**, *131*, 265.
(34) Albrecht, T.; Moth-Poulsen, K.; Christensen, J. B.; Hjelm, J.; Bjornholm, T.; Ulstrup, J. *J. Am. Chem. Soc.* **2006**, *128*, 6574.
(35) Datta, S.; Tian, W. D.; Hong, S. H.; Reifenberger, R.; Henderson, J. I.; Kubiak, C. P. *Phys. Rev. Lett.* **1997**, *79*, 2530.
(36) Mujica, V.; Roitberg, A. E.; Ratner, M. *J. Chem. Phys.* **2000**, *112*, 6834.
(37) Kornyshev, A. A.; Kuznetsov, A. M.; Ulstrup, J. *Proc. Natl. Acad. Sci. U.S.A.* **2006**, *103*, 6799.
(38) Voityuk, A. A.; Siriwong, K.; Rosch, N. *Angew. Chem., Int. Ed.* **2004**, *43*, 624.
(39) Chi, Q. J.; Farver, O.; Ulstrup, J. *Proc. Natl. Acad. Sci. U.S.A.* **2005**, *102*, 16203.
(40) van Zalinge, H.; Schiffrin, D. J.; Bates, A. D.; Haiss, W.; Ulstrup, J.; Nichols, R. J. *ChemPhysChem* **2006**, *7*, 94.